



HAL
open science

A unique electrical resistivity experiment reveals the 3D interior of Piton de la Fournaise

Lydie Gailler, Romain Guillard, Solène Buvat, Philippe Labazuy, Anthony Finizola, Emilie Roulleau, Jean-François Lénat, Cyril Aumar, Guillaume Boudoire, Baptiste Camus, et al.

► To cite this version:

Lydie Gailler, Romain Guillard, Solène Buvat, Philippe Labazuy, Anthony Finizola, et al.. A unique electrical resistivity experiment reveals the 3D interior of Piton de la Fournaise. *Scientific Reports*, 2025, 15 (1), pp.35794. <10.1038/s41598-025-17161-4>. <hal-05333700>

HAL Id: hal-05333700

<https://hal.science/hal-05333700v1>

Submitted on 27 Oct 2025

HAL is a multi-disciplinary open access archive for the deposit and dissemination of scientific research documents, whether they are published or not. The documents may come from teaching and research institutions in France or abroad, or from public or private research centers.

L'archive ouverte pluridisciplinaire HAL, est destinée au dépôt et à la diffusion de documents scientifiques de niveau recherche, publiés ou non, émanant des établissements d'enseignement et de recherche français ou étrangers, des laboratoires publics ou privés.



Distributed under a Creative Commons CC BY-NC-ND 4.0 - Attribution - Non-commercial use - No Derivative Works - International License



OPEN A unique electrical resistivity experiment reveals the 3D interior of Piton de la Fournaise

Lydie Gailler¹✉, Romain Guillard¹, Solène Buvat¹, Philippe Labazuy¹, Anthony Finizola^{2,3}, Emilie Roulleau^{2,4,5}, Jean-François Lénat¹ & The ERT3D Scan4Volc team*

Understanding the internal structure of volcanoes is essential for improving predictions of eruptions and for assessing hazards. However, creating high-resolution models of their interiors remains a significant challenge. At Piton de la Fournaise, we conducted an innovative 3D electrical resistivity tomography to produce a new high-resolution image of the subsurface beneath the Terminal Cone, extending down to 1 km below the summit. Our model not only images a large hydrothermal zone beneath the layered lava flows, but also reveals conductive offshoots extending toward the surface beneath the Bory crater and along faults linked to the Dolomieu crater. These findings suggest that hydrothermal activity is strongly influenced by volcano-tectonic features at the summit. This study provides valuable insights into fluid circulation, magma transfer, and instability, offering a new framework for understanding the present structure of Piton de la Fournaise and proposes a novel approach for studying the spatio-temporal evolution of volcanoes worldwide.

Keywords Piton de la Fournaise, 3D electrical resistivity experiment, High resolution modeling, Hydrothermal system, Preferential fluid path

Our understanding of volcano dynamics relies directly on the quality of our knowledge of the location, nature and geometry of the magmatic and hydrothermal systems, and of mechanical heterogeneities. Imaging this internal structure at a sufficiently high resolution is a great challenge, but is essential for identifying the internal dynamic processes that govern the overall volcanic phenomena. In this context, two fundamental questions condition our future ability to quantify the spatio-temporal evolution of volcanoes:

- (i) How to spatially image volcanic reservoirs, preferential magmatic and hydrothermal paths, as well as mechanical heterogeneities in 3D?
- (ii) What are the causal relations between such a complex internal structure inferred from geophysical signals and the surface manifestations directly observed in the field?

This study aims to answer these questions using innovative tools applied to volcano imaging.

Imaging the internal structure of a volcanic edifice presents specific issues due to the complexity of its evolution, where numerous phenomena are interconnected in space and time. These include the recharge and emptying of magma reservoirs, the development of hydrothermal activity, eruptive and intrusive processes, and volcano-tectonic events (such as fracturing, caldera formation, flank collapse, and sliding). As a result, volcanic structures are among the most complex geological structures, and it is not always easy to establish the relationships between active structures at depth and the eruptive manifestations at the surface. In addition, it may be impossible to collect scientific data from key areas due to inaccessibility (e.g. rugged topography, fault zones) or the hazards that they pose (e.g. eruptive activity, dangerous gas emanations, unstable zones). The field conditions may require careful adaptation of the experimental protocol. This involves conducting preliminary surveys to test the instruments, to plan their optimal theoretical deployment according to field accessibility, and performing first order synthetic numerical simulations to assess the resolution expected for different configurations of the sensors.

¹Laboratoire Magmas et Volcans, Université Clermont Auvergne, CNRS, IRD, OPGC, Clermont-Ferrand, France.

²Laboratoire GéoSciences Réunion, Université de La Réunion, 97744 Saint Denis, France. ³Université de Paris, Institut de physique du globe de Paris, CNRS, 75005 Paris, France. ⁴Stratagem974, 97490 Sainte Clotilde, France.

⁵BRGM La Réunion, 5 rue Ste Anne, 97490 St Denis, France. *A list of authors and their affiliations appears at the end of the paper. ✉email: lydie.gailler@uca.fr

Our study focuses on Piton de la Fournaise volcano, located on La Réunion Island (Fig. 1a), one of the most famous volcano laboratories in the world. Highly active and closely monitored by the Observatoire Volcanologique du Piton de la Fournaise of Institut de Physique du Globe de Paris (OVPF-IPGP), this edifice is an ideal place to experiment with new methodologies aimed at integrating spatio-temporal modeling of volcanic dynamics. This ‘4D’ approach requires the construction of a detailed initial state model (carried out in this work) whose dynamics can then be monitored by means of additional but less frequent and widely dispersed iterative measurements.

Within the Enclos Fouqué caldera (Fig. 1b), the Piton de la Fournaise Terminal Cone is a highly complex and heterogeneous structure. Its summit comprises craters and pit-craters (Bory,- Pre-Bory, Dolomieu, Soufrière, Petit Plateau), and is intensely fractured due to successive inflation/deflation periods, collapse events, and intrusions. At depth, there are highly active hydrothermal and magmatic reservoirs^{1–3}, where the shallow depth (i.e. > 1 km AMSL) volcano-tectonic seismicity is mainly concentrated, associated with magma transport and shallow reservoir pressurization⁴. Three main preferential zones for the opening of eruptive fissures originate from the Terminal Cone: the southeast rift zone (SERZ), the northeast rift zone (NERZ), and the 120 N rift zone (N120 or NW-RZ). Photos are presented in Supplementary Material A to illustrate these specific areas and the associated results described below (Fig. 3a).

The knowledge to date of its internal structure was summarized by⁵ who compiled all available geological and geophysical information along an E-W profile crossing the main active part of the edifice (Fig. 1c). This latter has been built and evolves in response to various types of volcanic and volcano-tectonic activities. The main ones include: (1) frequent eruptive activity associated with dikes and sills of different geometries depending on the path taken in the shallow feeder system^{3,6}, (2) a hydrothermal system below the Terminal Cone which has caused 17 phreatomagmatic eruptions within the Dolomieu crater since the eighteenth century⁷, and (3) an

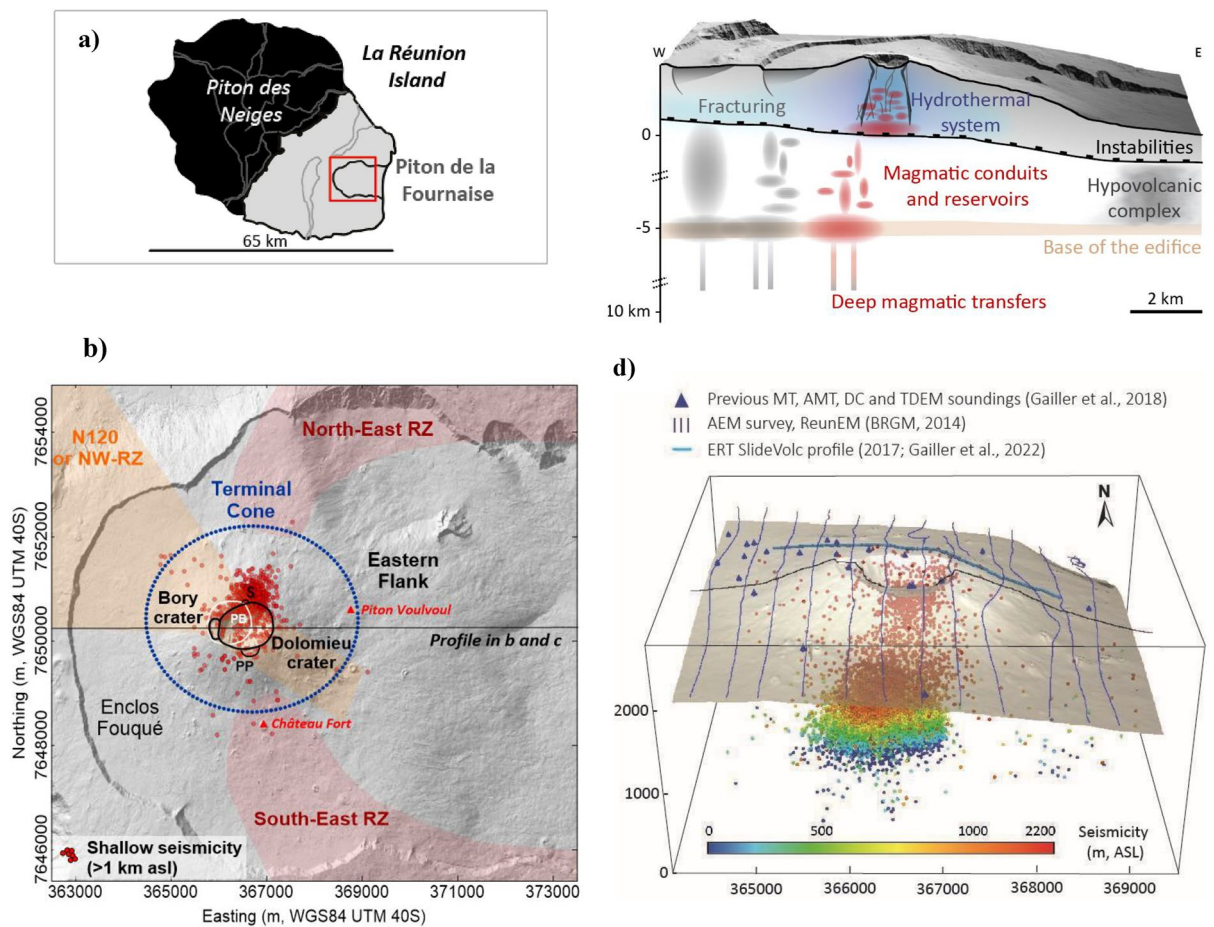


Fig. 1. The overall context of Piton de la Fournaise and state of the art of its inner structure. **(a)** Location of Piton de la Fournaise (La Réunion Island, Indian Ocean). **(b)** Focus on the main area discussed in text and shallow depth seismicity (2016–2021, OVPF-IPGP, doi: <https://doi.org/10.18715/REUNION.OVPF>). S: Soufrière, PP: Petite Plateau, PB: pre-Bory pit-crater. **(c)** Detailed inner structure along the EW profile crossing the central part of Dolomieu Crater inferred from geophysical studies (located in b; see Lénat et al., 2012 for details). **(d)** Distribution of all available previous electrical and electromagnetic surveys at the scale of the study area (i.e. the Terminal Cone), superimposed onto the seismicity shown in b).

active sliding plane beneath the eastern flank^{6,8}, where large displacements have been observed (several meters over the last few decades). In the past, large eastward flank landslides occurred^{9,10}, generating tsunamis^{11–13}.

The edifice has been the subject of numerous geophysical investigations over the past years (see¹⁴ and references therein). Our work focuses on the electrical resistivity structure of the Terminal Cone. This parameter, very sensitive to fluid content, is well suited to imaging the structure of a volcanic edifice as it detects conductive regions such as magmatic or hydrothermal systems, the water table and fractured or altered zones. Several methods exist to probe the distribution of electrical resistivity at various depths and scales depending on the equipment, its geometry in the field, and the resistivity values of the subsurface (Fig. 1d):

- 1D vertical approaches, such as electrical soundings, Time Domain ElectroMagnetism (TDEM) and Audio-MagnetoTelluric (AMT) soundings for fairly shallow investigations, and Magnetotelluric (MT) soundings for deeper investigations of more than 10 km (blue triangles in Fig. 1d).
- 2D Electrical Resistivity Tomography (ERT) which reaches down to about 600 m in depth along a specific profile¹⁵, as has been shown for various volcanic contexts.

In addition, a large-scale helicopter-borne electromagnetic campaign (ReunEM, BRGM¹⁶; dark blue lines in Fig. 1d) was conducted in 2014, collecting high density 1D measurements along parallel lines spaced 500 m apart, which were used to create a pseudo-3D global resistivity model of Piton de la Fournaise down to depths of 400 to 600 m below the surface. However, the resolution of measurements obtained by these methods is still insufficient for a detailed 3D investigation of the volcano's interior at depths greater than 600 m. The pathways of fluid transfer from magmatic and hydrothermal reservoirs to the surface are strongly influenced by the inherited structure of the edifice, which requires more precise imaging. Consequently, enhancing the resolution of these structures is essential for a better understanding of the edifice's evolution and its potential impact on future activity. The aim of this study was to generate a deeper, high-resolution 3D resistivity model of the edifice using an innovative strategy that provides more detailed information than previous geophysical surveys, particularly the work of Dumont et al.¹⁶ using the same parameter (resistivity).

We present here the results of a unique 3D ERT of the Terminal Cone of Piton de la Fournaise using an innovative approach carried out for the first time in such a large and complex environment (i.e. large surface area: covering more than 13 km²; with significant topographical difficulties: steep slopes and complicated flow morphologies). We used the recently developed © IRIS Fullwaver system technology¹⁷ that was adapted to overcome the considerable field limitations while ensuring full 3D acquisition with an excellent investigation resolution laterally and at depth (Fig. 2a). For comparison in terms of resolution, our final dataset includes 885-3D signals, compared to 240-1D soundings in Dumont et al.¹⁶ for an area of 10 km². Details of the experimental device are presented in the Material and Methods sections and Supplementary Material B, which goes into greater depth about the scientific challenges inherent in such an experiment (Fig. 2b).

A 3D animation of the overall model presented in Fig. 3a is provided in Supplementary Material C. Qualitatively, the main limitations of this model in terms of spatial resolution arise from the spacing between the reception electrodes and the distribution of the mobile current electrodes, which were evenly distributed across the field. We also encountered some difficulties in injecting a current in such a highly resistive environment, but intensity was fairly uniform, ensuring consistent measurements over the whole study area. The depth of investigation is especially influenced by the distance of the remote fixed current electrode in this pole-dipole configuration, with a decrease in resolution at depth commonly observed with this ERT approach. In terms of the data distribution at depth (Fig. 3a), the current experimental design provides reliable homogeneous 3D coverage of the Terminal Cone, as further detailed in the Methods-Experimental Design section.

Results

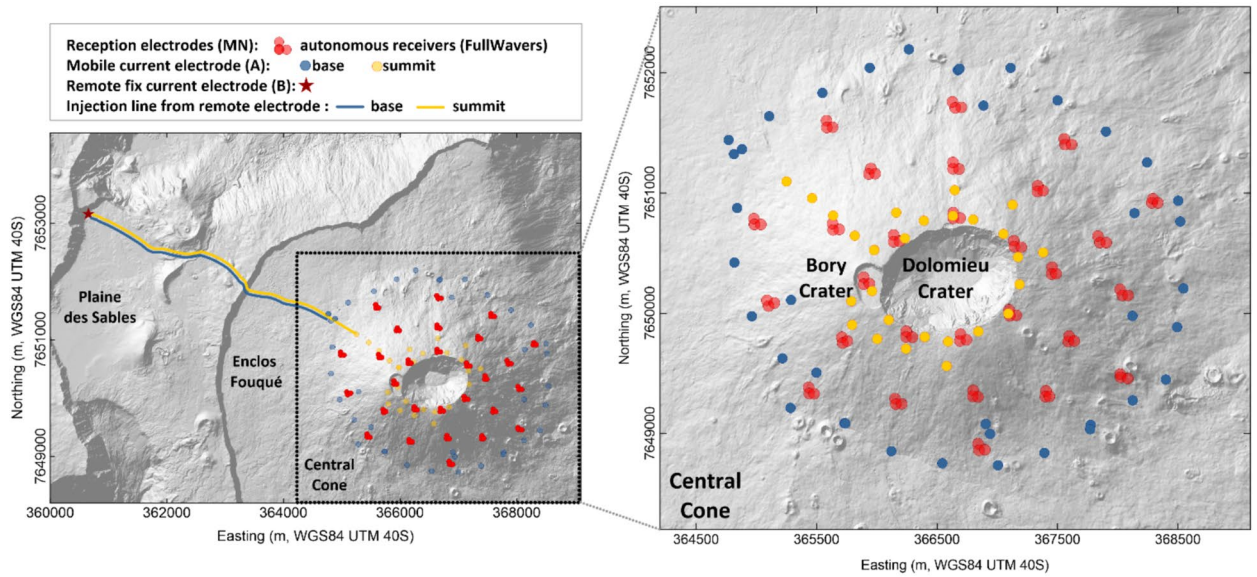
Qualitative overview of the 3D resistivity model

Here we focus on the associated shallow structures (i.e. the first km of the edifice) that are influenced by the magmatic, hydrothermal and mechanical dynamics as a whole. The 3D resistivity model shows, to the first order, the classical, very long wavelength resistivity distribution commonly found at Piton de la Fournaise^{16,18,19}, as well as in similar volcanic contexts, such as Kilauea volcano²⁰. A shallow, high resistivity layer (from 1000 to more than 10,000 Ω.m) of varying thickness (between 200 and 500 m on average) is associated with the massive lava flows observed at the surface. It overlies a large, lower resistivity body (<500 Ω.m) imaged here with an unprecedented resolution, revealing fine, previously unknown details of its uppermost layers. In this context, a conductive body of this type is unequivocally identified as the hydrothermal system surrounded by alteration and with fluid injections toward the surface, with a complex interplay between fluid saturation, alteration processes and mineralization (see Pereira et al. 2024 and references therein).

Although this value is higher than resistivity values commonly observed for hydrothermal systems on other volcanoes, comparison between our Fig. 3b with the highest self-potential (SP) values (i.e. maxima produced by electrokinetic phenomena on active volcanoes) shown on the map of the Piton de la Fournaise Terminal Cone (Fig. 4 in Barde-Cabusson et al.²¹) strongly suggest that our lower resistivity values are associated with rising hydrothermal fluids. Similar hydrothermal system signatures, comparing SP and ERT, have already been found in other active volcanic contexts (for example at Stromboli, Revil et al.²²). Quantitatively, since it is impossible to sample the hydrothermal system at depth, the model therefore only show resistivity contrasts. Accordingly, it seems acceptable to consider these lower resistivity values (<500 Ω.m) at Piton de la Fournaise volcano as corresponding to the hydrothermal system, fluids circulation and associated alteration at various depths.

Other local resistivity contrasts (500–1000 Ω.m) are observed in certain places, which are associated with known and/or suspected geological and volcano-tectonic features at various scales, as detailed in the following analysis along the main slices.

a)



b)

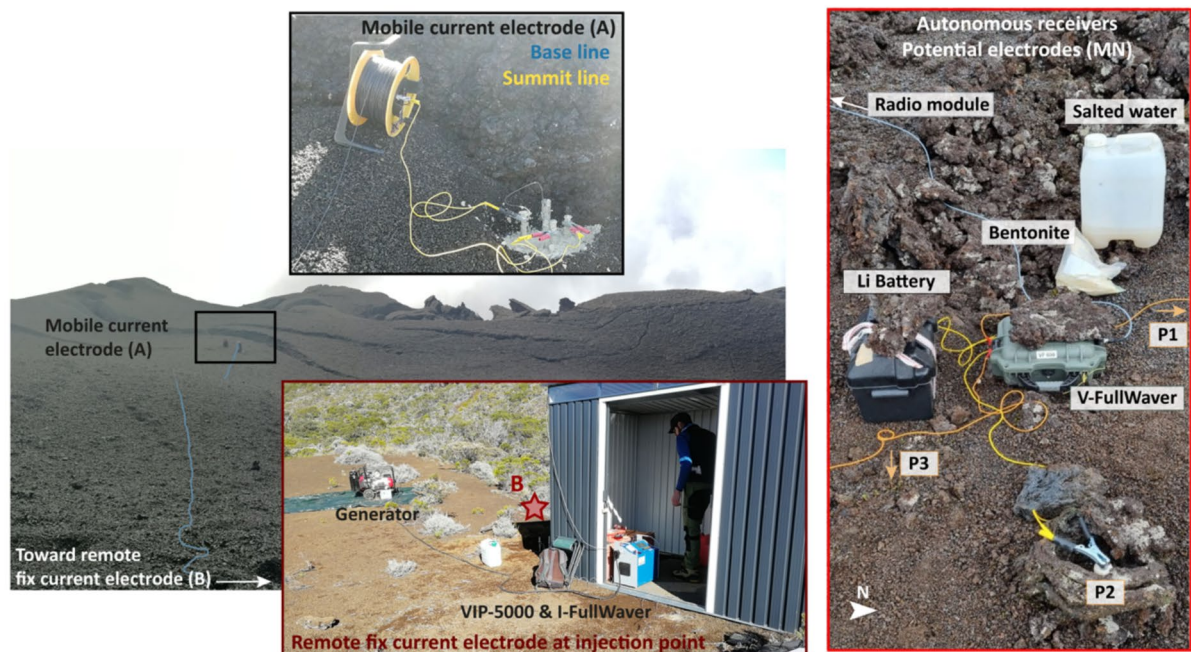


Fig. 2. The 3D experiment at Piton de la Fournaise using FullWaver design (© Iris Instruments). **(a)** Distribution of the investigation multi-electrodes array (5 m resolution LIDAR DEM, acquired in 2009/11 ©IGN2010 and updated by Structure From Motion - OVPF, coordinates are given in meters within system WGS84-UTM 40S). **(b)** Photos of the equipment used in the field (© the Scan4Volc team).

Detailed analysis along main slices

The horizontal slice at 1800 m AMSL (about 400 m below the base of the cone; Fig. 3b) illustrates the geometry of the main low resistivity body. It extends laterally over more than 2 km with a NW–SE elongation following the orientation of the N120 RZ. Also at this depth, a curvilinear resistive structure oriented toward the sea appears below the eastern flank. Similar but slightly less resistive structures can also be seen in the axes of the NE and SE rift zones.

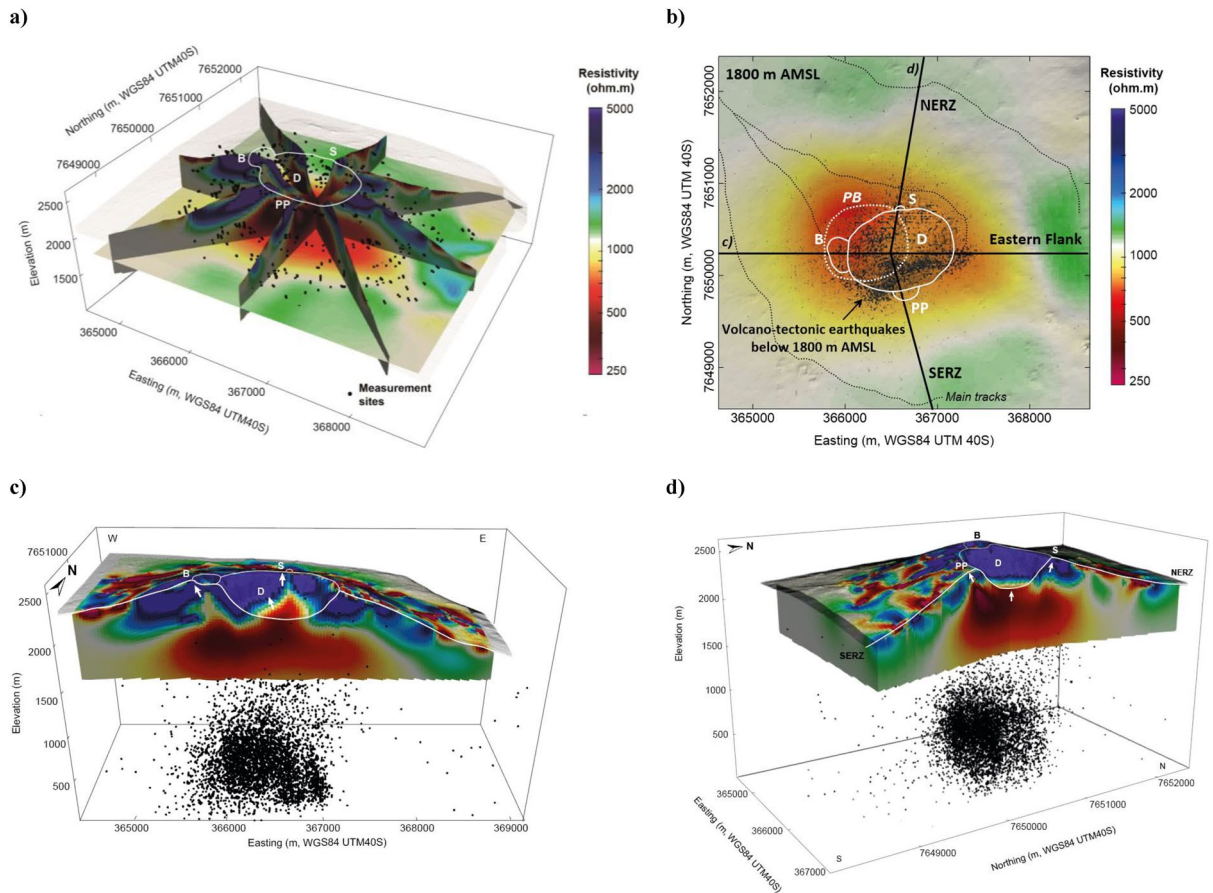


Fig. 3. The new 3D resistivity model of Piton de la Fournaise Terminal Cone. **(a)** Visualization of the overall 3D model through selected slices, location of measurement sites (black dots) and main summit areas of interest (they are located by their initials in **b** and **c**—B; Bory crater; D: Dolomieu crater; S: Soufrière; PP: Petit Plateau; SERZ: South-East rift zone; NERZ: North-East rift zone). **(b)** Location of the two main slices presented in **c**) on a horizontal slice within the 3D resistivity model at 1800 m AMSL. **(c,d)** E-W and N-S slices, respectively, within the 3D resistivity model crossing the main area of interest, as described in the text (see Supplementary Material A for field evidences). White arrows locate the main hydrothermal ascents to the surface. In **(b–d)**, the distribution of volcano-tectonic earthquakes (OVPF-IPGP, doi: <https://doi.org/10.18715/REUNION.OVPF>) is represented by black dots.

Along the W-E slice crossing the summit craters and the eastern flank (Fig. 3c), several sub-vertical discontinuities dissect the shallow, massive, resistive flows. Locally, the model highlights elongated low resistivity lenses at the surface, especially to the west of Bory crater and at the easternmost part of the slice. Although we cannot rule out that these surface variations are due to measurement artifacts (due to electrode coupling), they could also be related to fracturing since the model statistics demonstrate a high level of confidence in these measurements. On the eastern flank, which is known to be less stable⁶, the model reveals block discontinuities as discussed hereafter. Below the resistive layers, the conspicuous large, low-resistivity body, identified as the main zone occupied by the hydrothermal system, is marked by two protuberances rising towards the surface below Dolomieu and Bory craters. At depth, the lowest values of resistivity are located around an elevation of 2000 m AMSL (that is 100–200 m below the floor of the Enclos Fouqué caldera), and the resistivity tends to increase regularly with depth.

We evidence additional features along the N-S slice crossing the outer NE and SE rift zones along which most of the magmatic injections are concentrated (Fig. 3d). An offshoot of the low resistivity body coincides with the highly altered area of the Soufrière pit-crater. We also note a low resistivity channel rising towards the surface in the area of the so-called Petit Plateau, a pit-crater that formed and was active in 1791 before being filled by lava flows. Further away from the summit, the NE rift zone appears to be more conductive than the SE one at shallow depth.

Finally, we note that most of the shallow volcano-tectonic seismicity⁴ is concentrated beneath the inferred hydrothermal system, except for the shallowest hypocenters associated with magma injections (in particular to the north for the period considered here). The lateral extension of this main seismic zone at depth coincides fairly well with that of the low resistivity body.

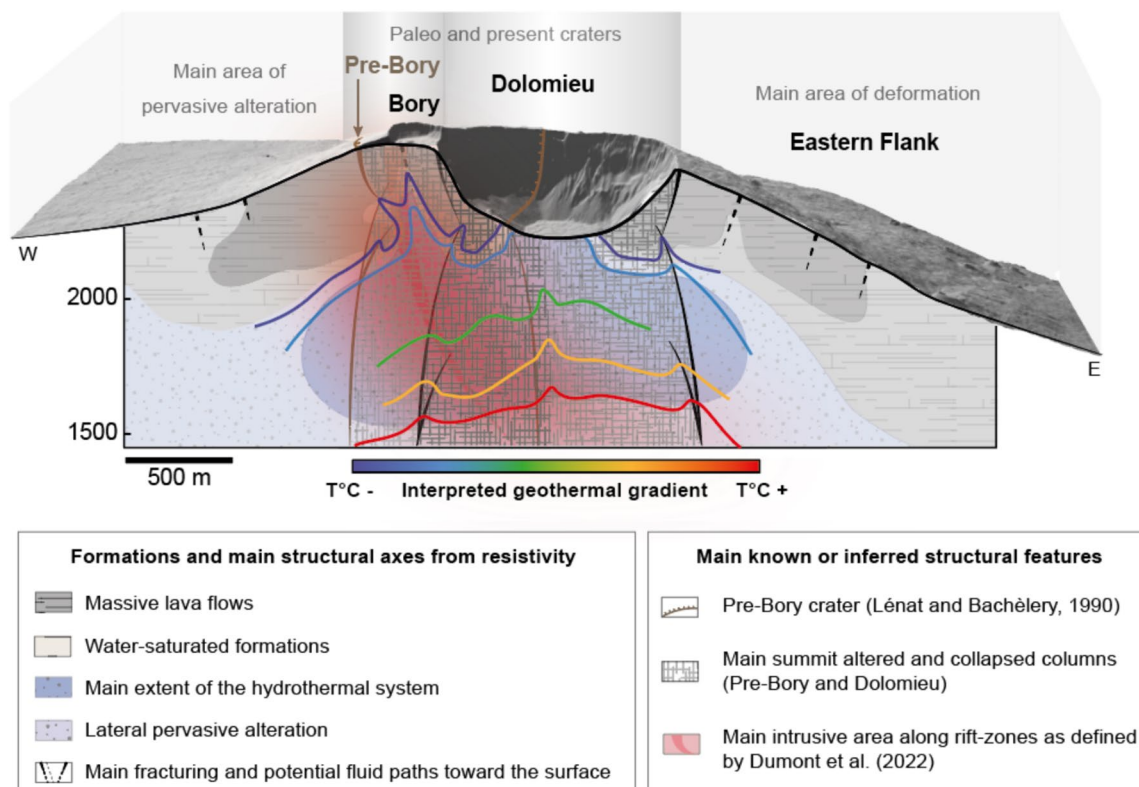


Fig. 4. Detailed reference model of Piton de la Fournaise inner structures. Interpretation in terms of future dynamics, from direct 3D electrical resistivity investigation.

Discussion

This new geophysical model highlights the complexity and heterogeneity of Piton de la Fournaise's Terminal Cone at an unprecedented horizontal and vertical resolution (Fig. 4). It allows the distribution of resistivity to be resolved, and hence the different lithologies interpreted in detail and in an overall consistent way (Fig. 3c and d). It provides new information regarding the structure and evolution of the edifice, and supersedes the pseudo 3D resistivity model obtained from helicopter-borne measurements interpreted by Ref¹⁶. and the 2D model of Ref⁵.

We provide a detailed image of the high resistivity lava flows that composed the Terminal Cone, which are clearly visible in the walls of the Dolomieu crater following its collapse of about 350 m in 2007^{23,24}. According to our model, the shell of water-unsaturated lava flows, characterized by their very high resistivity, reaches 500 m in thickness (Fig. 3c and d). This is consistent with the hydrogeological model of²⁵ which postulated that the top of the water table was at a similar depth. However, as described above, the model shows that this highly resistive pile of lava flows is dissected by low resistivity axes and zones rising toward the surface. In such a highly active eruptive context, this could also be explained by the presence of numerous eruptive fissures on the flanks of the cone, which have generated fractures in the lava pile and may have induced alteration of the medium through the channeling of hot fluids.

At depth, the 3D geometry of the low resistivity body interpreted as a zone deeply altered by hydrothermal activity has now been clearly imaged, with a considerably improved resistivity distribution compared to previous models. The successive collapses in the summit zone from the historical period onward, such as that in 2007^{26,27}, and probably well before, imply the existence of a composite column of brecciated and fractured rocks at depth beneath the summit area, extending down to the magma reservoir zone. We show here that the main part of the hydrothermally altered zone lies within this column. The low resistivity body below Dolomieu crater almost outcrops at the bottom of the new 350 m-deep crater, with ascents identified near the center of the crater and along its peripheral faults (Fig. 4). Those along the crater walls coincide with the large thermal and degassing anomalies observed after the 2007 collapse^{23,26}. The protrusion in the center of the crater may be an inherited structural feature since it coincides with the Pre-Bory crater boundary. Moreover, the Pre-Bory crater, a circa 700 m-diameter filled pit crater, is easy to observe in the western wall of the Dolomieu crater (Supplementary Material A) at about 150 m below the present surface. The presence of such a large collapse in this area suggests the emptying of an underlying magma reservoir²⁸.

A feature that had also not been resolved by previous models is that of a large and well-defined rise of the low resistivity body beneath Bory crater, which⁵⁴ would not be anticipated since the latter crater is far less active than the Dolomieu one. However, Bory crater is known to have been a major center of activity in the eighteenth century, with lava lake activity. Another phenomenon that might also be involved in the development of hydrothermal activity below the Bory crater is the large number of magmatic injections that propagated in

this area⁶. This is also in good agreement with the upward flow of hydrothermal fluids inferred in the same area by a positive SP anomaly²¹. This preferential upward path of hydrothermal fluids under the Bory crater (as well as under the Dolomieu crater) has also been highlighted by analysis of SP temporal surveys from 1993 to 2008, and by multi-scale wavelet tomography (MWT^{29,30}). Smaller areas that collapsed in the past (Petit Plateau, La Soufrière; Fig. 3c) also appear as zones with higher hydrothermal activity within the Terminal Cone.

Below 2000 m AMSL, the observed trend of increasing resistivity with depth could be linked to a decrease in model resolution due to lower data constraints at depth, reducing sensitivity to deeper, fine-scale conductive structures, and higher inversion smoothing with a possible overestimation of resistivity values.

However, it might also be a real factor, since this type of distribution is commonly observed in high temperature geothermal systems as evidenced by Refs^{31,32}, where the resistivity structure is characterized by a low resistivity cap overlying a more resistive core. As temperature increases with depth, a succession of different mineralogical assemblages are observed, explaining the increase in resistivity (from the zeolite-smectite zone toward the chlorite-epidote one, as also proposed by Darnet et al.³³). Therefore, the resistivity structure of the hydrothermal system could be interpreted in terms of a geothermal gradient, and one of the most striking features is the shape of the iso-resistivity contours that provide important new structural information (i.e. defining the main structural boundaries) in terms of mechanical weaknesses at depth.

The consistency between the extent of the low resistivity body and the main seismic zone suggests that the hydrothermal system was created and is fed by heat and fluids rising from the magma reservoir, which is inferred to be situated at about sea level^{34,35} in a zone that is highly fractured by magma injections^{6,28}. We also note that the virtual lack of seismicity within the low resistivity body may suggest a medium that is not prone to fracturing.

Although the low resistivity zone is mainly located beneath the summit craters, it clearly extends over a larger area, as also proposed by Ref⁷. Beyond the summit area, the lower resistivity of the eastern flank compared to the western one is attributed to a larger concentration of volcanic cones and eruptive fissures on the eastern flank and at the base of the cone, along the N120/NW–SE direction³⁶, which could be related to a main axis of thermal activity. This higher magmatic activity implies greater deformation of the eastern flank, with a dominant eastward component of horizontal deformation⁶, tending to increase conductivity through fracturing that favors fluid circulation toward the surface. A higher concentration of intrusions is also proposed along the less resistive narrow path of the NERZ compared to the SERZ (Fig. 3d).

Therefore, this study confirms that the detection of resistivity anomalies is a powerful tool for imaging volcanic systems at various scales. The complex inner structure imaged here confirms the general asymmetric magma-induced pattern of deformation proposed by Ref³⁷, with a strong effect of rock heterogeneity on magmatic injection paths and hydrothermal alteration axes.

The presence of low-resistivity structures suggests hydrothermal alteration and fluid circulation, influencing various phenomena and hazards. These include phreatic explosions, large-scale ductile deformation, porosity contrasts, gas emissions, seismicity distribution, magmatic intrusion pathways, vertical collapses, and horizontal displacements.

Since the dynamics of active volcanoes involve continuous changes in their internal structure at various depths, our results are highly promising for tracking these internal variations over time. This new high-resolution model can provide an initial step toward spatio-temporal (i.e. 4D) monitoring.

Although ERT cannot be easily repeated on such a large 3D scale, the model effectively captures the current internal state of Piton de la Fournaise and provides its first-order structure over a lateral extent of 4 km and down to a depth of 1 km. In addition to fundamental parameters collected in real-time by the volcano observatory (primarily seismicity and deformation), rapid and complementary approaches can be deployed to offer valuable and timely insights into the volcano's evolution. These approaches include 1D magnetotelluric monitoring³⁸, high-resolution 3D magnetization models based on repeated UAV magnetic field measurements³⁹, continuous time-series monitoring of the magnetic field⁴⁰, and self-potential measurements²¹, all strategically located over potential preferential fluid circulation paths highlighted by the ERT model. It is important to note that such an approach coupling ERT with SP, or using SP alone, has already made it possible to locate important eruptive crises in advance (Piton de la Fournaise, 2007 and Stromboli 2002–2003), down to a meter-scale, to locate fracturing or volcano collapses^{41,42}. In this general scheme, the current ERT structural model provides a background context, enabling us to construct a model which can be added to over time by means of an integrated volcano monitoring approach, which we find highly promising.

Methods

Experimental design

The 3D electrical resistivity FullWaver system at the Laboratoire Magmas et Volcans (CAPRICE project, FEDER Auvergne) was developed and designed by IRIS Instruments for quadrupoles in a pole-dipole configuration (see Supplementary material A; Fig. S1). The combination of the receivers and the transmitter forms a Resistivity Distributed Automated System (R-DAS), with a measurement principle similar to that used for multi-electrode resistivity meters. It consists of measuring the current injected by the transmitter between two current electrodes and the resulting voltage between two receiver electrodes^{43,44}.

We initially planned the theoretical positioning of the experimental design using Fullwave Designer (Iris Instruments) in order to ensure the most homogeneous 3D cover of the Terminal Cone based on a detailed statistical analysis of the layout of the theoretical measurements (see Statistical analysis below). In the year before the survey we carefully assessed the rough topography and accessibility of the measurement sites, the logistics in terms of transport of material to the site, the schedule for installation, measurements, removal and return transportation of equipment. Then, once in the field, we slightly adjusted the overall measurement positions, in order to optimize our investigation of the edifice geometry.

Reducing ground contact resistance in such a lava-resistant environment was also a significant challenge, carefully controlled at each receiver and each injection point. This fundamental logistical step enabled the resistance to be reduced considerably from 900 to 20 Ω on average at the receiver dipoles, and in the range 10–20 kohm between the injection and remote electrodes, allowing a current of between 50 to 150 mA to be injected. In terms of acquisition parameters, the total injection time was set to 60 s, corresponding to 12–13 stacks for a 2 s injection duration. Also note that the whole full-waveform acquisition at 100 Hz favors the removal of noise during data processing.

Another major point was the accuracy of the electrode positioning, which is also a key factor in assessing the uncertainty of the dataset. Given the field conditions and the volume of equipment already involved, we chose to carry out the positioning using the Differential GNSS mode on Garmin GPSMAP 67. Measurements were performed at each electrode site for at least 2 min, and then post-treated using the software TOPCON TOOLS, using the 6 closest permanent GNSS stations belonging to the OVPP-IPGP as reference points. We estimate the accuracy on each position to be in the range 0.3 to 0.4 m and 0.3 to 0.5 m in the horizontal and vertical planes, respectively.

Statistical and data analysis

In practice, 64 injections were recorded by 28 triplets of measurements spread out on a 4×4 km² surface area around the Dolomieu crater (about 500 m from each other; Fig. 2a), i.e. 84 electrodes distributed, as planned, all around the edifice despite the difficult field access. The electrode spacing for potential measurements was 50 m. The final 3730 signals recorded, of various quality, were analyzed in detail, and saturated and very small magnitude signals were removed (<0.04 mV) for which the resistivity could not be calculated. For the low and noisy signals, we performed careful filtering using a Fourier series and cardinal sine processing specially developed in order to recover most of the signals while removing noise within the time series. In the end, 31% of signals recorded (a total of 1150) were usable. Conspicuous spikes observed in the injection signals were also removed to provide a fully filtered dataset. Additional details on data analysis and filtering are provided in Supplementary Material A (Sect. 2).

Data processing and inversion

We used ERTLAB software, which is based on a three-dimensional finite element method and an L2-norm (smoothness constraint) for the misfit function. The software uses the preconditioned conjugate gradient method^{46–48} with a symmetric successive over-relaxation (SSOR) preconditioner. Noise was appropriately managed using a robust data weighting algorithm^{49,50}.

Spatial discretization was used, with a mesh of hexahedrons which could successfully treat the complex topography of the terrain⁵¹, and forward modeling was performed using mixed boundary conditions (Dirichlet and Neumann). The main area of interest, called the “foreground region” (Fig. S3), was discretized with 30 m \times 30 m \times 30 m cell size, in other words a little over half the electrode spacing, to ensure good accuracy for the model. Beyond the foreground region, a large background region was designated to mitigate boundary effects. It had cells of increasing size (from 60 to 240 m in size), extending about 2 km to the S-E and included the remote electrode to the N-W. It enabled the exact location of the remote electrode to be included during the processing^{52,53}.

The starting model was set with a homogeneous apparent resistivity of 1120 Ω .m (i.e. median value of apparent resistivities from statistical analysis) and a noise rate of 10%. The inversion process was driven by modeling parameters summarized in Tab. S1 and led to a final inverse model of resistivity whose forward solution best fitted measured data to a predetermined noise level. The convergence of the inversion process from the constructed starting model was achieved after 10 iterations with a correct fit of the model: 4.3% of data exhibited residuals of more than 2 sigma (see residuals distribution in Supplementary material A “Data analysis and filtering” section).

Data availability

3D resistivity model is available at <https://doi.org/10.25519/W9J6-TD91>.

Received: 19 December 2024; Accepted: 21 August 2025

Published online: 14 October 2025

References

1. Derrien, A., Villeneuve, N. & Peltier, A. Monitoring volcanic activity with multi-scale 4D mapping. (2017).
2. Lénat, J. F. & Bachèlery, P. Dynamics of magma transfers at Piton de la Fournaise volcano (Réunion Island, Indian Ocean). In: Chi-Yu & Scarpa, R. (eds) *Earth Evol. Sci. Special Issue 'Modeling of volcanic processes'*, Friedr. Vieweg & Sohn, Braunschweig/Wiesbaden. 57–72 (1988).
3. Peltier, A., Staudacher, T. & Bachèlery, P. New behaviour of the Piton de La Fournaise volcano feeding system (La Réunion Island) deduced from GPS data: Influence of the 2007 Dolomieu caldera collapse. *J. Volcanol. Geotherm. Res.* **192**, 48–56 (2010).
4. Duputel, Z. *et al.* Seismicity of La Réunion island To cite this version : Comptes Rendus Géoscience. (2021).
5. Lénat, J. F., Bachèlery, P. & Merle, O. Anatomy of Piton de la Fournaise volcano (La Réunion, Indian Ocean). *Bull. Volcanol.* **74**, 1945–1961 (2012).
6. Dumont, Q., Cayol, V., Froger, J. & Peltier, A. major destabilization structure revealed by 22 years of satellite imagery at Piton de la Fournaise. *Nat. Commun.* <https://doi.org/10.1038/s41467-022-30109-w> (2022).
7. Villeneuve, N. & Bachèlery, P. Review of volcanic eruption typology at the Piton de la Fournaise, processes and hazards. *Cybergeo Eur. J. Geogr.* <https://doi.org/10.4000/cybergeo.2536> (2006).
8. Poland, M. P., Peltier, A., Bonforte, A. & Puglisi, G. The spectrum of persistent volcanic flank instability: A review and proposed framework based on Kilauea, Piton de la Fournaise, and Etna. *J. Volcanol. Geotherm. Res.* **339**, 63–80 (2017).

9. Labazuy, P. Instabilités au cours de l'évolution d'un édifice volcanique en domaine intraplaque océanique: le Piton de la Fournaise (Ile de la Réunion). Approche pluridisciplinaire à partir des données de campagnes marines. (Thèse d'Université, Univ. Blaise Pascal, 1991).
10. Labazuy, P. Recurrent landslides events on the submarine flank of Piton de la Fournaise volcano (Réunion Island). In: McGuire, W., Jones, A. P. & Neuberg, J. (eds) *Volcano Instability on the Earth and other Planets*. 293–305 (Geol. Soc. Spec. Publ. London, 1996).
11. Paris, R., Ramalho, R. S., Madeira, J., Ávila, S. & Matthias, S. Megatsunami conglomerates and flank collapses of ocean island volcanoes. *Mar. Geol.* **395**, 168–187 (2017).
12. Paris, R., Kelfoun, K. & Giachetti, T. MARINE CONGLOMERATE AND REEF MEGACLASTS AT MAURITUS ISLAND: Evidences of a tsunami generated by a flank collapse of the PITON DE LA Fournaise volcano, Reunion Island?. *Sci. Tsunami Hazards* **32**, 281–291 (2013).
13. Kelfoun, K., Giachetti, T. & Labazuy, P. Landslide-generated tsunamis at Réunion Island. *J. Geophys. Res.* **115**, 17 (2010).
14. Gailler, L. S. & Lénat, J. F. Internal architecture of La Réunion (Indian Ocean) inferred from geophysical data. *J. Volcanol. Geotherm. Res.* <https://doi.org/10.1016/j.jvolgeores.2012.01.015> (2012).
15. Gailler, L. et al. Volcano-magnetic signal reveals rapid evolution of the inner structure of Piton de la Fournaise. *J. Geophys. Res. Solid Earth* **128**, 1–14 (2023).
16. Dumont, M. et al. Imagery of internal structure and destabilization features of active volcano by 3D high resolution airborne electromagnetism. *Sci. Rep.* **9**, 1–11 (2019).
17. Gance, J., Leite, O., Texier, B., Bernard, J. & Truffert, C. The Fullwaver systems : Distributed network of autonomous devices for deep 3D electrical resistivity and induced polarization survey. *Egu* **20**, 12569 (2018).
18. Gailler, L.-S., Martí, A. & Lénat, J.-F. Complex structure of Piton de la Fournaise and its underlying lithosphere revealed by magnetotelluric 3D inversion. *J. Volcanol. Geotherm. Res.* <https://doi.org/10.1016/j.jvolgeores.2018.03.006> (2018).
19. Lénat, J. F., Fitterman, D. & Jackson, D. B. Geoelectrical structure of the central zone of Piton de la Fournaise volcano (Réunion). *Bull. Volc.* **62**(2), 75–89 (2000).
20. Gailler, L. et al. 3D electrical conductivity imaging of Halema'uma'u lava lake (Kilauea volcano). *J. Volcanol. Geotherm. Res.* **381**, (2019).
21. Barde-Cabusson, S. et al. Structural control of collapse events inferred by self-potential mapping on the Piton de la Fournaise volcano (La Réunion Island). *J. Volcanol. Geotherm. Res.* **209–210**, 9–18 (2012).
22. Revil, A. et al. Hydrogeology of Stromboli volcano, Aeolian Islands (Italy) from the interpretation of resistivity tomograms, self-potential, soil temperature and soil CO₂ concentration measurements. *Geophys. J. Int.* **186**, 1078–1094 (2011).
23. Staudacher, T. Field observations of the 2008 summit eruption at Piton de la Fournaise (Ile de La Réunion) and implications for the 2007 Dolomieu collapse. *J. Volcanol. Geotherm. Res.* **191**, 60–68 (2010).
24. Urai, M., Geshi, N. & Staudacher, T. Size and volume evaluation of the caldera collapse on Piton de la Fournaise volcano during the April 2007 eruption using ASTER stereo imagery. *Geophys. Res. Lett.* **34**, L22318 (2007).
25. Join, J. L., Coudray, J. & Longworth, K. Using principal components analysis and Na/Cl ratios to trace groundwater circulation in a volcanic island: the example of Réunion. *J. Hydrol.* **190**, 1–18 (1997).
26. Peltier, A., Massin, F., Bachèlery, P. & Finizola, A. Internal structure and building of basaltic shield volcanoes: The example of the Piton de La Fournaise terminal cone (La Réunion). *Bull. Volcanol.* **74**, 1881–1897 (2012).
27. Gailler, L. et al. Gravity structure of Piton de la Fournaise volcano and inferred mass transfer during the 2007 crisis. *J. Volcanol. Geotherm. Res.* **184**, 31–48 (2009).
28. Michon, L., Ferrazzini, V. & Di Muro, A. Magma paths at Piton de la Fournaise Volcano. In *Active Volcanoes of the Southwest Indian Ocean: Piton de la Fournaise and Karthala* (eds Patrick, B. et al.) 91–106 (Springer, 2016).
29. Mauri, G., Saracco, G., Labazuy, P. & Williams-Jones, G. Correlating hydrothermal system dynamics and eruptive activity—A case-study of Piton de la Fournaise volcano, La Réunion. *J. Volcanol. Geotherm. Res.* **363**, 23–39 (2018).
30. Saracco, G., Labazuy, P. & Moreau, F. Localization of self-potential sources in volcano-electric effect with complex continuous wavelet transform and electrical tomography methods for an active volcano. *Geophys. Res. Lett.* **31**, 1–5 (2004).
31. Nono, F. et al. Electrical conductivity of Icelandic deep geothermal reservoirs up to supercritical conditions: Insight from laboratory experiments. *J. Volcanol. Geotherm. Res.* **391**, (2020).
32. Árnason, K., Karlsdóttir, R., Eysteinnsson, H., Flóvenz, Ó. G. & Thor, S. The resistivity structure of high-temperature geothermal systems in Iceland. *Proc. World Geotherm. Congr.* **2000**, 923–928 (2000).
33. Darnet, M. et al. Geophysical signature of the transition zone between the sedimentary cover and the basement: An analogue approach to help de-risking geothermal prospects. *Eur. Geother. Congress* <https://doi.org/10.48550/arXiv.1905.07897> (2019).
34. Peltier, A., Bachèlery, P. & Staudacher, T. Magma transport and storage at Piton de La Fournaise (La Réunion) between 1972 and 2007: A review of geophysical and geochemical data. *J. Volcanol. Geotherm. Res.* **184**, 93–108 (2009).
35. Lénat, J.-F. et al. Structure and morphology of the submarine flank of an active basaltic volcano : Piton de la Fournaise (Réunion Island, Indian Ocean). *Oceanol. Acta* **10**, 211–223 (1990).
36. Michon, L., Ferrazzini, V., Di Muro, A., Villeneuve, N. & Famin, V. Rift zones and magma plumbing system of Piton de la Fournaise volcano: How do they differ from Hawaii and Etna?. *J. Volcanol. Geotherm. Res.* **303**, 112–129 (2015).
37. Letourneur, L., Peltier, A., Staudacher, T. & Gudmundsson, A. The effects of rock heterogeneities on dyke paths and asymmetric ground deformation: The example of Piton de la Fournaise (Réunion Island). *J. Volcanol. Geotherm. Res.* **173**, 289–302 (2008).
38. Wawrzyniak, P., Zlotnicki, J., Sailhac, P. & Marquis, G. Resistivity variations related to the large March 9, 1998 eruption at La Fournaise volcano inferred by continuous MT monitoring. *J. Volcanol. Geotherm. Res.* **347**, 185–206 (2017).
39. Gailler, L., Labazuy, P., Régis, E., Peltier, A. & Ferrazzini, V. Active structures and thermal state of the Piton de la Fournaise summit area revealed by combined UAV magnetic and IR measurements. *Volcanica in press*, (2022).
40. Zlotnicki, J., Delmond, J. C., Pambrun, C. & Delorme, H. Magnetic variations on Piton de la Fournaise volcano . Volcanomagnetic signals associated with the November 6 and 30 , 1987, eruptions. **56**, (1993).
41. Finizola, A., Aubert, M., Revil, A., Schütze, C. & Sortino, F. Importance of structural history in the summit area of Stromboli during the 2002–2003 eruptive crisis inferred from temperature, soil CO₂, self-potential, and electrical resistivity tomography. *J. Volcanol. Geotherm. Res.* **183**, 213–227 (2009).
42. Chaput, M. et al. Where does a volcano break? Using self-potential reiteration to forecast the precise location of major destructive events on active volcanoes: the case study of the Piton de la Fournaise 2007 caldera collapse. *Volcanica* **2**, (2019).
43. Carrier, A., Fischanger, F., Gance, J., Cocchiara, G., Morelli, G., Lupi, M., 2019. Deep electrical resistivity tomography for the prospection of low- To medium-enthalpy geothermal resources. *Geophys. J. Int.* **219**, 2056–2072. <https://doi.org/10.1093/gji/ggz411>
44. Lajaunie, M., Gance, J., Nevers, P., Malet, J.P., Bertrand, C., Garin, T., Ferhat, G., 2019. Structure of the Séchilienne unstable slope from large-scale three-dimensional electrical tomography using a Resistivity Distributed Automated System (R-DAS). *Geophys. J. Int.* **219**, 129–147. <https://doi.org/10.1093/gji/ggz259>
45. Peltier, A., Chevrel, M. O., Harris, A. J. L. & Villeneuve, N. Reappraisal of gap analysis for effusive crises at Piton de la Fournaise. *J. Appl. Volcanol.* **11**, 1–17 (2022).
46. Ellis, R.G., Oldenburg, D.W., 1994. Applied geophysical inversion. *Geophys. J. Int.* **116**, 5–11.
47. Spitzer, K., 1995. A 3-D finite-difference algorithm for DC resistivity modelling using conjugate gradient methods. *Geophys. J. Int.* **123**, 903–914. <https://doi.org/10.1111/j.1365-246X.1995.tb06897.x>

48. Zhang, J., Mackie, R.L., Madden, T.R., 1995. 3-D resistivity forward modeling and inversion using conjugate gradients. *Geophysics*, **60**, 1313–1325.
49. LaBrecque, D.J., Ward, S.H., 1990. Two-Dimensional Cross-Borehole Resistivity Model Fitting, in: *Geotechnical and Environmental Geophysics: Volume III*, Geotechnical. Society of Exploration Geophysicists. <https://doi.org/10.1190/1.9781560802785.3.ch4>
50. Morelli, G., Labrecque, D.J., 1996. Advances in ERT inverse modeling. *Eur. J. Environ. Eng. Geophys.* **1**, 171–186.
51. Fischanger, F., Catanzariti, G., Comina, C., Sambuelli, L., Morelli, G., Barsuglia, F., Ellaithy, A., Porcelli, F., 2019. Geophysical anomalies detected by electrical resistivity tomography in the area surrounding Tutankhamun's tomb. *J. Cult. Herit.* **36**, 63–71. <https://doi.org/10.1016/j.culher.2018.07.011>
52. Razafindratsima, S., Lataste, J.F., 2014. Estimation of the error made in Pole-Dipole Electrical Resistivity Tomography depending on the location of the remote electrode: Modeling and field study. *J. Appl. Geophys.* **100**, 44–57. <https://doi.org/10.1016/j.jappgeo.2013.10.008>
53. Robain, H., Albouy, Y., Dabas, M., Descloitres, M., Camerlynck, C., Mechler, P., Tabbagh, A., 1999. The location of infinite electrodes in pole–pole electrical surveys: consequences for 2D imaging. *J. Appl. Geophys.*, **41**, 313–333. [https://doi.org/https://doi.org/10.1016/S0926-9851\(99\)00010-5](https://doi.org/https://doi.org/10.1016/S0926-9851(99)00010-5)
54. Michon, L., Muro, A. Di, Villeneuve, N., Saint-marc, C., Fadda, P., Manta, F., Michon, L., Muro, A. Di, Villeneuve, N., Saint-marc, C., Fadda, P., 2013. Explosive activity of the summit cone of Piton de la Fournaise volcano (La Réunion island) : A historical and geological review. <https://doi.org/10.1016/j.jvolgeoes.2013.06.012>

Acknowledgements

The seismic and GNSS data presented in this paper were collected by Observatoire Volcanologique du Piton de la Fournaise, Institut de Physique du Globe de Paris (OVPF-IPGP, doi: <https://doi.org/10.18715/REUNION.OVPF>). We thank the Service National d'Observation en Volcanologie (SNOV, CNRS-INSU) for the use of the database. We thank the OVPF-IPGP's staff, and the Parc National de La Réunion for their support all along this project. A special and warm acknowledgement is dedicated to all the co-workers, all the volunteers, Aurélie de Bernardy de Sigoyer, Alain Bertil, Oryaëlle Chevrel, Allan Derrien, Messie Dupont, Michel Frangieh, Juliette Jolivet, Cédric Laborde, François Lötter, François Martel, Arthur Vaitilingom, Nicolas and Rafael Vinet Roulleau, for their precious contribution to this survey. We also thank IRIS Instruments, Julien Gance, Orlando Leite, for their advice and support all along this experiment, and InXpress Auvergne, Yassine Bensouda for logistic support. Photos taken in the heart of the Parc National de La Réunion with the authorization of the establishment of the Park. 3D resistivity inversion was performed using ERTlab software and associated representations were generated thanks to Paraview software. Filtering was carried out using dedicated Matlab codes.

Author contributions

Conceptualization and supervision: L.G., P.L., A.F., J.F.L., E.R. Methodology: L.G., S.B., R.G., P.L., A.F., J.F.L., E.D. Field investigation: all authors Data filtering and modeling: L.G., S.B., R.G., Q.D., E.T. Visualization: L.G., R.G., S.B., P.L., A.F., E.R., J.F.L. Writing—original draft: L.G., S.B., R.G., J.F.L. Writing—review & editing: all authors.

Funding

This work was financially supported:—Agence National Research project Scan4Volc: <https://anr.fr/Project-ANR-21-CE49-0015>.—CNES in the framework of the projects Volcadrone & RMagEDrone: “Imagerie géophysique multi-échelles des édifices volcaniques”.—FEDER Auvergne and AELB for the purchase of the FullWaver equipment. This is contribution no. 692 of the ClerVolc program of the International Research Center for Disaster Sciences and Sustainable Development of the University of Clermont Auvergne. CASUD project, Université de La Réunion.

Declarations

Competing interests

The authors declare no competing interests.

Additional information

Supplementary Information The online version contains supplementary material available at <https://doi.org/10.1038/s41598-025-17161-4>.

Correspondence and requests for materials should be addressed to L.G.

Reprints and permissions information is available at www.nature.com/reprints.

Publisher's note Springer Nature remains neutral with regard to jurisdictional claims in published maps and institutional affiliations.

Open Access This article is licensed under a Creative Commons Attribution-NonCommercial-NoDerivatives 4.0 International License, which permits any non-commercial use, sharing, distribution and reproduction in any medium or format, as long as you give appropriate credit to the original author(s) and the source, provide a link to the Creative Commons licence, and indicate if you modified the licensed material. You do not have permission under this licence to share adapted material derived from this article or parts of it. The images or other third party material in this article are included in the article's Creative Commons licence, unless indicated otherwise in a credit line to the material. If material is not included in the article's Creative Commons licence and your intended use is not permitted by statutory regulation or exceeds the permitted use, you will need to obtain permission directly from the copyright holder. To view a copy of this licence, visit <http://creativecommons.org/licenses/by-nc-nd/4.0/>.

© The Author(s) 2025

The ERT3D Scan4Volc team

Cyril Aumar¹, Guillaume Boudoire¹, Baptiste Camus⁶, Nicolas Cluzel¹, Eric Delcher^{2,3}, Quentin Dumont⁹, Rachel Gusset², Laurent Métral⁶, Aline Peltier^{3,7}, Laurent Perrier⁴, Léopold Poussin⁴, Edouard Régis⁸, Thierry Souriot¹, Erwan Thébault¹, Diego Tobías López¹⁰ & Nicolas Villeneuve^{2,3}

⁶Univ. Grenoble Alpes, Univ. Savoie Mont Blanc, CNRS, IFSTTAR, 38000 Grenoble, IRDISTerre, France. ⁷Institut de Physique du Globe de Paris, Observatoire Volcanologique du Piton de la Fournaise, 97418 La Plaine des Cafres, France. ⁸Observatoire de Physique du Globe de Clermont, Université Clermont Auvergne, CNRS, Clermont-Ferrand, France. ⁹Institute of Seismology and Volcanology, Faculty of Science, Hokkaido University, North 10 West 8, Kita-ku, Sapporo, Hokkaidō 060-0810, Japan. ¹⁰Instituto de Ciencias de la Tierra, Universidad de El Salvador (UES), San Salvador, El Salvador.